IEEE Access
Multidisciplinary | Rapid Review | Open Access Journal

Received November 13, 2019, accepted December 4, 2019, date of publication December 12, 2019,
date of current version December 23, 2019.

Digital Object Identifier 10.1109/ACCESS.2019.2959088

A New Control Strategy for SR Generation System Based on Modified PT Control

XIAOSHU ZAN[1], KAI NI[2], (Student Member, IEEE), WENYUAN ZHANG[1], ZHIKAI JIANG[1], MINGLIANG CUI[3], DONGSHENG YU[1], (Member, IEEE), AND RONG ZENG[4], (Member, IEEE)

[1]School of Electrical and Power Engineering, China University of Mining and Technology, Xuzhou 221008, China
[2]School of Electrical and Electronic Engineering, Huazhong University of Science and Technology, Wuhan 430074, China
[3]State Grid Dongtai County Electric Power Supply Company, Yancheng 224200, China
[4]Oak Ridge National Laboratory, Power Electronics and Electric Machinery Group, Knoxville, TN 37932, USA

Corresponding author: Kai Ni (nikai@hust.edu.cn)

ABSTRACT The Switched Reluctance generator (SRG) has been widely used as a constant voltage source due to its advantages of simple structure, low cost and high control flexibility. However, the output voltage ripples cannot be ignored due to its unique operating principle with phase commutation. In this paper, the influence of the control parameters on the output voltage ripples are analyzed, and a fly-wheeling pulse train (FW-PT) control strategy is proposed to suppress the voltage ripple. The output voltage can be regulated by the FW-PT control strategy by using two or more sets of preset control pulse combinations, therefore it has the advantages of simple circuit implementation, no Network compensation and fast response speed. The characteristics of steady-state and dynamic behaviors of the switched reluctance power generation system by using different control strategies are simulated and compared, and a platform of 200W 8/6 SRG is built for experimental verification. Simulation and experimental results confirm that compared with the traditional PID control strategy, the FW-PT control strategy can be used to not only suppress the output voltage ripple, but also achieve faster response and dynamic characteristics.

INDEX TERMS SR power generation system, pulse train, fly-wheeling current, voltage ripple, dynamic characteristics.

I. INTRODUCTION

A switched reluctance motor (SRM) has the advantages of simple structure, fault tolerance, high operating efficiency, strong mechanical characteristics, low temperature rise. Therefore, it has been widely used in wind power generation systems, aerospace, mining, textile and many other industrial scenarios [1]–[3]. An SRM can also operate as a generator by changing its control strategies for which, it is called a switched reluctance generator (SRG). An SRG has unique characteristics of no rotor windings, no brushes, and no permanent magnets. Hence, it can achieve low manufacturing cost, low copper consumption and high-power generation efficiency. In addition, the stators and rotors of SRG systems are controlled synchronously, and the stability of system can also be guaranteed even when the operating frequency is low [4]–[7]. However, the existence of large output voltage ripples degrades the power generation performance.

The associate editor coordinating the review of this manuscript and approving it for publication was Xiaodong Liang.

At present, many research efforts have been put on reducing the output voltage fluctuation and voltage stabilization of switched reluctance power generation systems (SRPGS). Aiming at suppressing the output voltage fluctuation of SRG, a previous paper [8] designed the filter to regulate the output voltage by optimizing the topological structure and parameters, which can effectively reduce the voltage harmonics. However, the parameters of filter are difficult to determine and the pressure building process is relatively long. In a previous paper [9], a sliding mode variable structure controller based on genetic algorithm optimization was designed, which focused on solving the voltage pulsation caused by factors such as speed of rotation and load changes during the operation process, but by introducing a genetic algorithm optimization module, it makes the system more complicated. Literature [10] achieves the effect of stable output voltage by changing the excitation voltage of the output voltage, which ignores the influence of other control quantities on the output voltage. In a previous paper [11], a digital control method was designed to use two preset pulse trains, which were combined with current chopping control to regulate

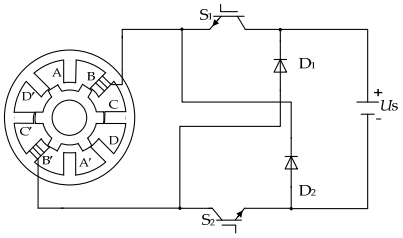

FIGURE 1. The 8/6 SRG profile.

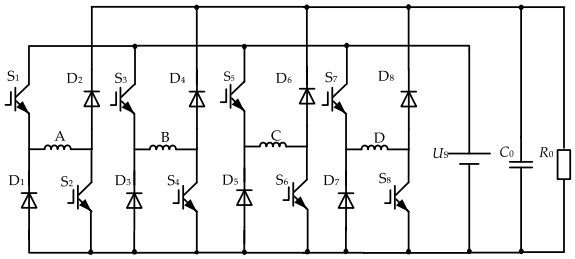

FIGURE 2. Excited asymmetrical half-bridge separately circuit.

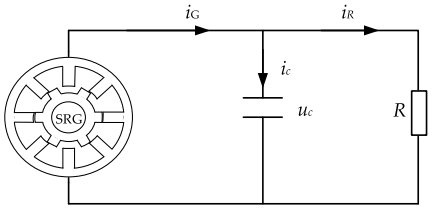

FIGURE 3. The flowing current of the SRG during power generation.

the SRPGS. It has better steady-state performance in the open-loop state, but ignores the dynamic performance of the power generation system. In paper [12], based on the analysis of pulse train (PT) control, a control method based on capacitive current is proposed, which is applied to the SRPGS to reduce the output voltage ripple. The feasibility of PT control used in SRPGS is verified. However, there is no in-depth analysis of the dynamic characteristics of SRPGS with PT control.

This paper focuses on the application of PT control used in SRPGS, based on which, a fly-wheeling pulse train (FW-PT) control for the SRPGS is proposed. The FW-PT control only adjusts the output voltage by two or more preset control pulse combinations, and has the advantages of simple circuit implementation, no network compensation and fast response [13]–[15]. In addition, this paper analyzes the voltage ripple of SRG and the influence of FW-PT control on the SRPGS when applying different parameters. Furthermore, the influence of load mutation on the voltage regulation is studied. The steady and dynamic characteristics of the SRPGS under different controls are analyzed. In the end, the simulation comparison analysis is carried out and an experiment platform of 200W 8/6 SRG is built for experimental verification.

II. ANALYSIS OF VOLTAGE FLUCTUATION OF SRG

A. SWITCHED RELUCTANCE POWER GENERATION SYSTEM

An SRG is a doubly salient varied reluctance motor, in which the convex sections of rotors and stators are laminated by ordinary silicon steel sheets [16], [17]. Figure 1 shows the schematic of a typical 4-phase 8/6 SRG.

When the generator is rotated clockwise to the position as shown in Figure 1, with S_1 and S_2 closed, the winding of phase A is excited by the power supply US. According to the principle of "the shortest magnetic circuit", the rotor is subjected to a counterclockwise torque, and the mechanical energy on the rotor is converted into magnetic energy, which is stored in the magnetic field. With S_1 and S_2 opened, the energy stored in the magnetic field is fed back to the power supply US through the circuit formed by D_1 and D_2, and the mechanical energy is converted into electric energy. Therefore, the SRG completes the conversion from mechanical energy to electrical energy.

The power converter circuit of the SR power generation system is mainly divided into self-excited and separately excited ones, which is selected according to actual conditions in practical applications. Figure 2 shows a typical four-phase asymmetric half-bridge circuit. This excitation mode can completely isolate the excitation power supply from the power generated by the windings, which has good controllability and stability [18].

B. ANALYSIS OF VOLTAGE FLUCTUATION

Due to the existence of nonlinear inductance, the irregular phase winding and parallel capacitance charges and discharges periodically, which leads to the fluctuation of the output voltage [19], [20]. The current flows from SRG during the power generation process is shown in Figure 3.

In the case of self-excitation, it can be derived as

$$i_c = C\frac{du_C}{dt} = C\frac{du_C}{d\theta}\omega_r \tag{1}$$

$$C\frac{du_C}{d\theta}\omega_r = i_G - i_R \tag{2}$$

where, i_G is the generator current.

The capacitance voltage u_c can be obtained from (1) and (2) as

$$u_C = C_1 e^{-\frac{\theta}{RC\omega_r}} - R\int_{\theta_{on}}^{\theta_{off}} i_G d\theta \tag{3}$$

where, θ_{on} is the conduction angle, θ_{off} is the turn off angle, and C_1 is the integral constant.

In the separately excited mode, when SRG operates in the fly-wheeling phase, the relationship of the currents is shown in (2), and when SRG is operated in the excitation phase, the capacitor is discharged. It can be expressed as

$$C\frac{du_C}{d\theta}\omega_r + i_R = 0 \tag{4}$$

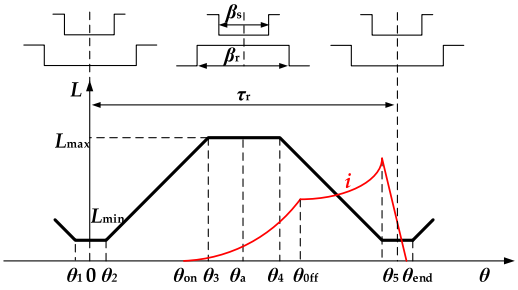

FIGURE 4. The typical phase current waveforms of the SRG.

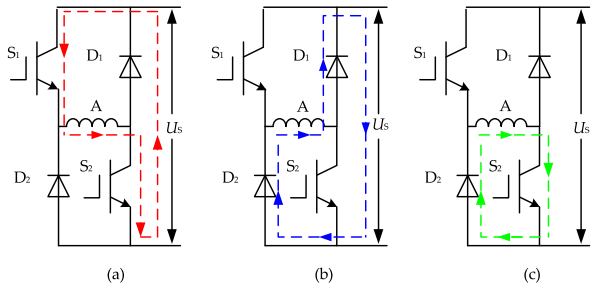

FIGURE 5. Operating states of switches under the chopper control.

The capacitance voltage u_c can also be achieved by

$$u_C = \begin{cases} C_2 e^{-\frac{\theta}{RC\omega_r}}, & \theta_{on} < \theta < \theta_{off} \\ C_3 e^{-\frac{\theta}{RC\omega_r}} - R\int_{\theta_{on}}^{\theta_{off}} i_G d\theta, & \theta_{off} < \theta < \theta_{end} \end{cases} \quad (5)$$

where, C_2 and C_3 are integral constants, and θ_{end} is the end angle of the freewheeling phase.

It can be seen from (3) and (5) that the output voltage u_c is mainly affected by the parameters R, C, θ_{on}, θ_{off}, and i_G.

III. FW-PT CONTROL

A. TRADITIONAL CONTROL OF SRG

Since the excitation and armature windings of an SRG are both stator windings, the excitation and power generation processes must adopt periodic time-sharing control. The excitation process is controllable, but at the same time, the power generation process is uncontrollable. Therefore, the power generation system is generally controlled by adjusting the excitation current. The traditional control methods of SRG can be generally divided into angular position control (APC), current chopping control (CCC) and pulse width modulation (PWM) [21], [22].

Figure 4 shows typical phase current waveforms of SRG. In the excitation phase ($\theta_{on} < \theta < \theta_{off}$), the excitation current is adjusted by controlling the on/off states of the switches and the output voltage is further adjusted.

Figure 5 shows the on/off states of the switches with voltage closed-loop PWM control. Figure 5a shows that the switches S_1 and S_2 are conducted, and at this moment, the DC source is used to excite the winding. When the output voltage (feedback voltage) is higher than the preset voltage, S_1 and S_2 are turned off. As shown in Figure 5(b), the winding current

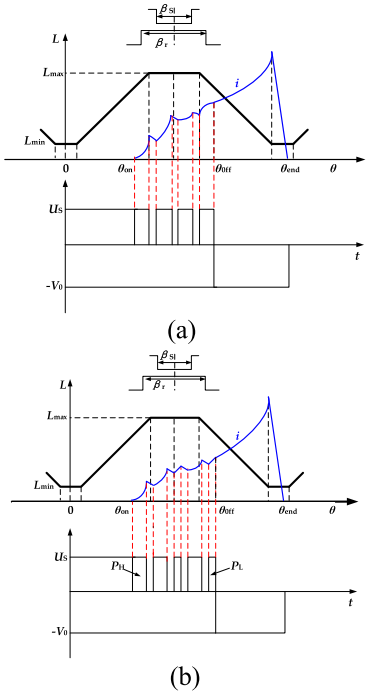

FIGURE 6. Waveforms of SR power generation system under (a) the traditional voltage closed-loop PWM and (b) PT control.

flows through the diodes D_1 and D_2. Thereby, the excitation current and the output voltage are reduced. Figure 5(c) shows that only the fly-wheeling circuit is active through D_2 and S_2, which is called soft chopping. At this stage, the flux linkage remains unchanged during the fly-wheeling chopping process.

Ignoring the voltage drop on the switches, the voltage across the winding of phase A can be expressed by

$$U_A = \begin{cases} U_S & S_1\text{on}, \quad S_2\text{on} \\ 0 & S_1\text{off}, \quad S_2\text{on} \\ -V_0 & S_1\text{off}, \quad S_2\text{off} \end{cases} \quad (6)$$

where, V_0 is the output voltage of SRG under separated excitation model.

B. FW-PT CONTROL OF SR POWER GENERATION SYSTEM

The traditional PT control adjusts the phase currents according to the relationship between the sampling and reference voltages, and adjusts the output voltage further. Compared with the conventional PID control, the PT control adjusts the output voltage by two or more preset control pulse combinations. Meanwhile, it has the advantages of simple circuit implementation, no network compensation and fast response. The waveforms of the SR power generation system under the traditional voltage closed-loop PWM and PT control are shown in Figure 6.

Figure 7(a) shows the waveforms of the output voltage of a typical 4-phase SR power generation system under voltage closed-loop PWM control. In the excited phase, the filter capacitor is periodically charged and discharged, and the

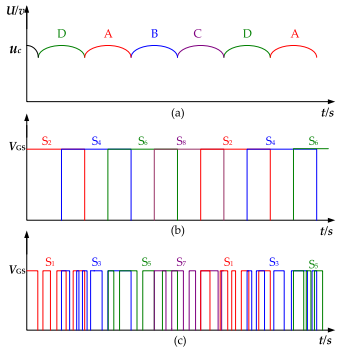

FIGURE 7. The waveforms of switches under the PWM control.

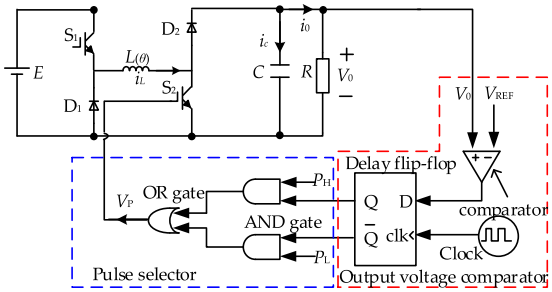

FIGURE 8. The SR power generation system with FW-PT control.

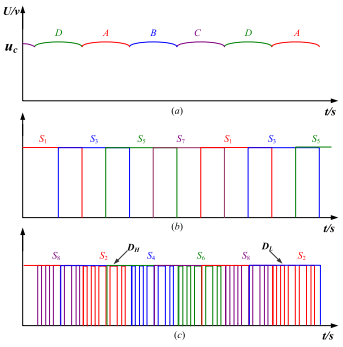

FIGURE 9. The waveforms of switches under the FW-PT control.

excitation voltage is changed by adjusting the duty cycle of PWM. Figures 7(b) and 7(c) show the triggering signals of the 4-phase switches. It can be seen from Figure 7 that when the rotor rotates to the conduction position of phase A winding ($\theta_{on} < \theta < \theta_{off}$), switch S_2 is turned on at this time, and the duty cycle of S_1 is adjusted according to the feedback voltage u_c. However, the excitation current of phase A is adjusted according to the voltage fluctuation caused by the freewheeling current of the phase D winding with the filter capacitor charging and discharging. By that analogy, it can be considered that the traditional control methods of the SRG, which control the excitation current, are hysteresis controls that control the fly-wheeling phase by indirectly adjusting the excitation current.

In order to solve the hysteretic control of the SR power generation system, this paper proposes a new method that

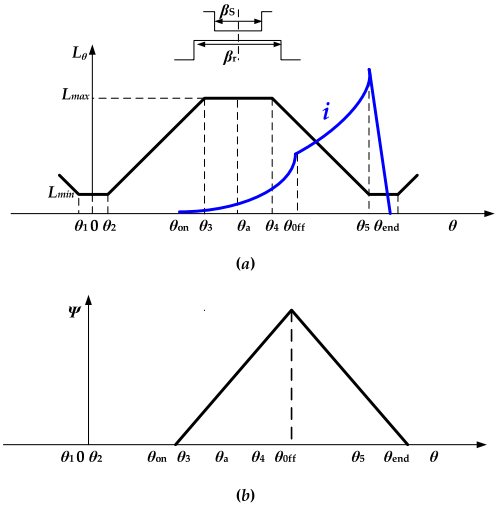

FIGURE 10. The waveforms of the phase current and flux linkage.

is called FW-PT control, which achieves an excellent effect on voltage ripple by controlling the pulse trains of the fly-wheeling phase.

Figure 8 is the schematic diagram of the SR power generation system with FW-PT control. Similar to PT control, FW-PT control selects the high and low duty cycles pulse trains by comparing the output voltage V_0 with the reference value V_{REF}. However, FW-PT control is only used in the fly-wheeling phase to control the fly-wheeling current. During the excited phase, the switches S_1 and S_2 are both turned on, and the phase windings are fully excited. Whereas, in the fly-wheeling phase, S_1 is turned off and S_2 is controlled according to the comparison of the output voltage V_0 and the reference value V_{REF}. When the lower switch S_2 is turned on, the winding current flows through S_2 and D_1 to form a freewheeling circuit, and the filter capacitor discharges the load and the output voltage drops. The output voltage can be maintained at a given value by switching the high and low duty cycle pulse trains.

Figure 9 shows the relevant waveforms with FW-PT control. It can be seen that high and low pulse trains are applied in the fly-wheeling phase. When the clock signal arrives, the output voltage V_0 and the reference value V_{REF} are compared, and the result of the comparison is sent to the delay flip-flop. Furthermore, when the output voltage V_0 is greater than the reference value, the output terminal Q of the delay flip-flop is 1 and $\bar{Q}$ is 0. Meanwhile, the high duty cycle pulse PH is selected as a control signal of S_2 through a logic OR gate circuit to reduce the output energy. Similarly, when the output voltage V_0 is smaller than the reference value, the output terminal Q of the delay flip-flop is 0 and $\bar{Q}$ is 1, Meanwhile, the low duty cycle pulse P_L is selected as a control signal of S_2 through a logic OR gate circuit to increase the output energy.

It can be seen from the above illustration that the on/off states of S_1 indicate the operating state (excitation or fly-wheeling) of the SR power generation system. When the SRG

is operating in the freewheeling phase, the output control pulse from the FW-PT controller is applied to S_2 to directly control the output voltage. The control pulse selection is expressed by

$$P = \begin{cases} P_{\mathrm{H}}, & V_0 \geq V_{\mathrm{REF}} \\ P_{\mathrm{L}}, & V_0 < V_{\mathrm{REF}} \end{cases} \tag{7}$$

Since the inductance value of the phase windings changes by the variation of θ, when SRG is operating in the fly-wheeling phase, during the conduction period of S_2, the phase current is raised nonlinearly. On the contrary, when S_2 is turned off, the phase current is decreased nonlinearly. Moreover, when the inductance current i_{L} is greater than the load current i_0, the inductance current i_{L} is used for supplying power to the load, the excess inductance current (i_{L}-i_0) is employed to charge the capacitor, and the output voltage can be increased. Conversely, when the inductance current i_{L} is smaller than the load current i_0, all the inductance current i_{L} is supplied to the load, the insufficient part of the required current (i_0-i_{L}) is supplemented by the capacitor discharge current (-i_{C}), and the output voltage drops.

It can be known from (7) that the pulse train selection of the FW-PT control is opposite to the conventional PT control.

Consequently, when the output voltage V_0 is greater than the reference value V_{REF}, the FW-PT control selects the high duty cycle pulse train PH. On the contrary, when the output voltage V_0 is smaller than the reference value V_{REF}, the FW-PT control selects the low duty cycle pulse train P_{L}.

C. THE ANALYSIS OF VOLTAGE RIPPLE UNDER FW-PT CONTROL

As shown in Figure 4, when the current is operated at phase (θ_{on}, θ_{off}), the current can be expressed by

$$i(\theta) = \frac{U_S(\theta - \theta_{on})}{\omega_r L(\theta)} \tag{8}$$

When the current is at phase (θ_{off}, θ_5), the current can also be obtained by

$$i(\theta) = \frac{u_c\,(2\theta_{\mathrm{off}} - \theta_{\mathrm{on}} - \theta)}{\omega_x \left[L_{\max} + \frac{dL}{d\theta}(\theta - \theta_4)\right.} \tag{9}$$

According to, $\psi(\theta) = L(\theta)^* i(\theta)$, the flux linkage can be written by

$$\psi = \begin{cases} \dfrac{U_{\mathrm{s}}\,(\theta - \theta_{\mathrm{on}})}{\omega_{\mathrm{r}}} & \theta_{\mathrm{on}} \leq \theta \leq \theta_{\mathrm{off}} \\ \dfrac{u_c\,(2\theta_{\mathrm{off}} - \theta_{\mathrm{on}} - \theta)}{\omega_{\mathrm{r}}} & \theta_{\mathrm{off}} \leq \theta \leq 2\theta_{\mathrm{off}} - \theta_{\mathrm{on}} \end{cases} \tag{10}$$

The relationship between phase current and flux linkage with rotor position θ is shown in Figure 10.

The voltage ripple amplitude can be obtained from (5), which can be expressed by

$$\Delta u = u_c\,(\theta_4)\left(e^{\frac{\theta - \theta_{\mathrm{off}}}{RC\omega_{\mathrm{r}}}} - 1\right) + \frac{\int_{\theta_4}^{\theta_5} i_{\mathrm{G}} d\theta}{\omega_{\mathrm{r}} C} \tag{11}$$

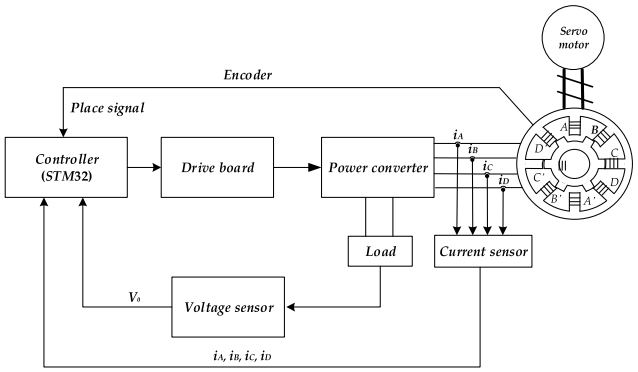

FIGURE 11. The control scheme of the 8/6 SRG system.

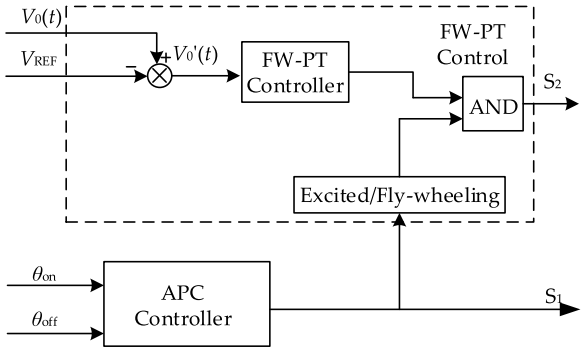

FIGURE 12. The flow chart of the FW-PT controller.

The voltage ripple can further be expressed as

$$\Delta u = \frac{1}{\omega_r C}\int_{\theta_{off}}^{\theta_5} i_G d\theta - \frac{P_0\left(\theta_{\max} - \theta_{off}\right)}{u_c \omega_r C} \tag{12}$$

where, P_0 is the output power, $\theta_{\max}$ is the position where the output voltage is largest.

It can be seen from (11) that as the time constant τ and the angular velocity ω_{r} increase, the voltage ripple Δu decreases. The smaller θ_{on} is and the larger θ_{off} is, the larger both the excited current and the voltage ripple will be.

D. THE DESIGN OF FW-PT CONTROLLER

Figure 11 is a structural diagram of a 4-phase 8/6 SR power generation system. During the voltage build-up phase, there is no control during the excitation phase, which ensures that the output voltage rises rapidly. In the cases of loading and unloading, the output voltage also has a conspicuous jump. The FW-PT controller mainly feeds back the output voltage as a state quantity to the controller. Through a reasonable control of the design parameters of the pulse trains of the fly-wheeling phase, the FW-PT controller ensures that the SRG can reach the rated voltage quickly without overshoot. In addition, by adjusting the duty cycle P_{H} and P_{L}, it is ensured that the system can achieve excellent control effects when loading and unloading are within a certain range. The working flow chart of the FW-PT controller is shown in Figure 12.

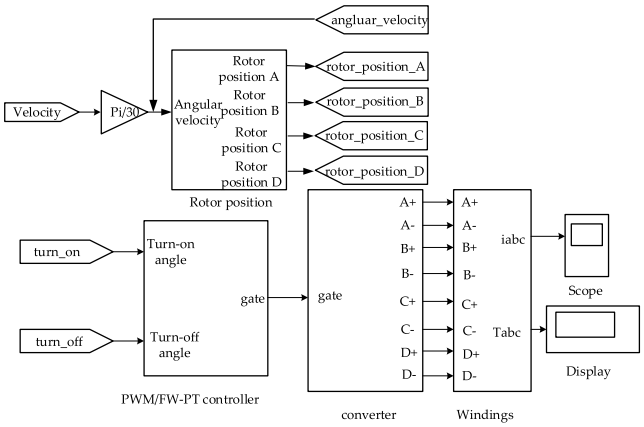

FIGURE 13. The simulation model of the 8/6 SR power generation system.

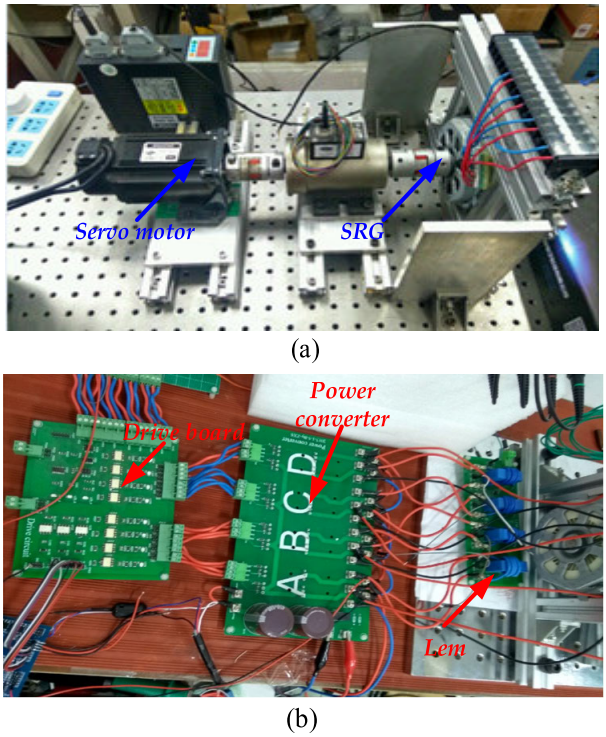

FIGURE 14. The photograph of the experiment platform of the SR power generation system; (a) Experiment platform of the SRG; (b) The control circuits and power converter.

IV. SIMULATION AND EXPERIMENTAL VERIFICATION

In order to verify the correctness of the theoretical analysis, based on the analysis of the SR power generation system and the FW-PT control, the simulation model of the 8/6 SRG shown in Figure 13 is built in the MATLAB/Simulink environment.

On the basis of simulation, the experimental platform of the SR power generation system shown in Figure 14 is also built by hardware design. The simulation and experimental parameters are shown in Table 1. The purpose of the simulation and experiment is to analyze the influence of the proposed control strategy on the operation performance of SRG, and compare the control effect of the FW-PT controller with the traditional PID controller from overshoot, response time and stability.

TABLE 1. The simulation and experimental parameters of the SR power generation system under the FW-PT control.

Parameters	Values	Parameters	Values
n, r/min	1200	P_H	0.85
θ_{on}, deg	15°	P_L	0.65
θ_{on}, deg	45°	R, Ω	12
U_S, V	50	C, uF	680
V_0, V	48	f, Hz	5000

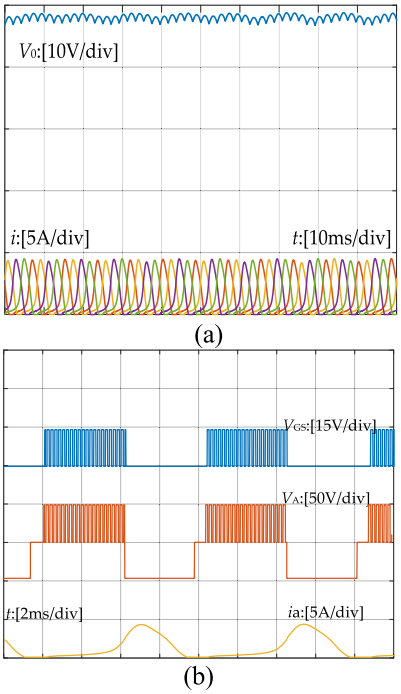

FIGURE 15. The simulation waveforms of SRG under the PID control; (a) The waveforms of output voltage V0 and phase currents; (b) The waveforms of control signal S1, voltage and current of phase A.

The starting process of the SR power generation system with FW-PT control can be summarized as: in the case of constant speed, the SRG starts, and the excitation section has no control effect and the voltage is quickly established. When the phase winding is operated in the fly-wheeling phase, the selection of the high pulse train P_H and no network compensation ensure that the overshoot does not appear during the process of establishing the voltage. In addition, real-time control of the output voltage is achieved by a reasonable selection of the duty cycle of the trigger signal.

Figure 15 shows the main simulation waveforms of the SR power generation system with traditional PID control at a constant speed. When the SR power generation system reaches a steady state, it can be seen from Figure 15(a), the output voltage reaches a given value of 48V, and its ripple is large. The waveform of the phase currents of the winding is in a steady state with the maximum value of 4A.

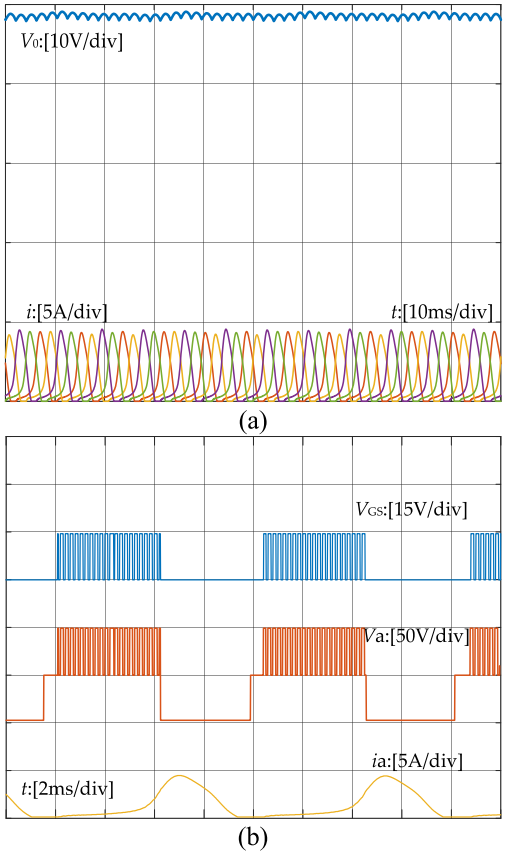

FIGURE 16. The simulation waveforms of SRG under the PT control; (a) The waveforms of output voltage V0 and phase currents; (b) The waveforms of control signal S1, voltage and current of phase A.

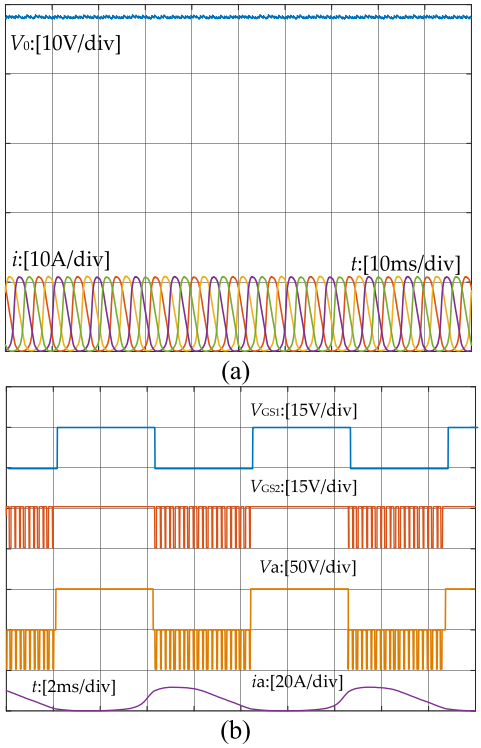

FIGURE 17. The simulation waveforms of SRG under the FW-PT control; (a) The waveforms of output voltage V0 and phase currents; (b) The waveforms of control signal S1, voltage current of phase A.

Figure 15(b) shows the simulation waveforms of control signal, phase voltage and phase-A current. With the control signals of S_1 and S_2, the voltage of phase A is changing in the excitation stage. When phase A is working in fly-wheeling stage, the phase voltage is 48V, which is the output voltage.

Figure 16 shows the main simulation waveforms of the SR power generation system with the traditional PT control. The high and low pulse trains have duty ratios of 0.8 and 0.6 respectively with a frequency of 5 kHz. Compared with the traditional PID control, when the system reaches a steady state, the output voltage V_0 is stabilized at 48V, but its ripple is large and reaches 1.2V, the waveform of the phase currents of the winding is in a steady state with the maximum value of 4A. It can be seen from Figure 16(b), with the change of output voltage, the controller chooses the control signal between P_H and P_L.

Figure 17 shows the main waveforms of SR power generation system with FW-PT control. The high and low pulse trains duty cycles are 0.85 and 0.65, respectively with the frequency of 5 kHz. With FW-PT control, after the system reaches the steady state, the output voltage V_0 is stabilized at 48V, and the ripple is about 0.5V. Compared with the traditional PI and PT controls, the voltage ripple in the case of FW-PT control is much smaller. Besides, the peak value of the phase current under the FW-PT control is about 12A. It can be seen from Figure 17(b) that at the excitation stage, S_1 and S_2 are fully on. The difference from other control methods is that the control signal of S_2 works at the fly-wheeling stage.

Figure 18 shows the voltage waveforms of the SR power generation system at the instants of starting and changing loads under the traditional PI, PT and the FW-PT controls. It can be seen that in the starting phase of the SR power generation system, the output voltage under the traditional PI control has a large overshoot, and reaches the steady state after about 0.06s. Whereas, with the traditional PT control, due to the limitation of preset duty cycle pulse and no network compensation, the output voltage has a smaller overshoot, and after about 0.04s, the system reaches a steady state, and the output voltage ripple is large, too. In addition, with FW-PT control, the system quickly establishes the output voltage due to the full conduction of switches during the excitation phase, and the steady state is reached after about 0.03s. Compared with the first two control methods, the output voltage ripple is smaller and the output voltage has no overshoot due to the limitation of the high duty cycle pulse in the fly-wheeling section.

At 0.1s, the load is changed from 12 Ω to 10 Ω. The output voltage in the case of PT control reaches the steady state after 0.01s, but the voltage ripple is larger than before, which indicates that the traditional PT control is not suitable for the SR power generation system under a variable load

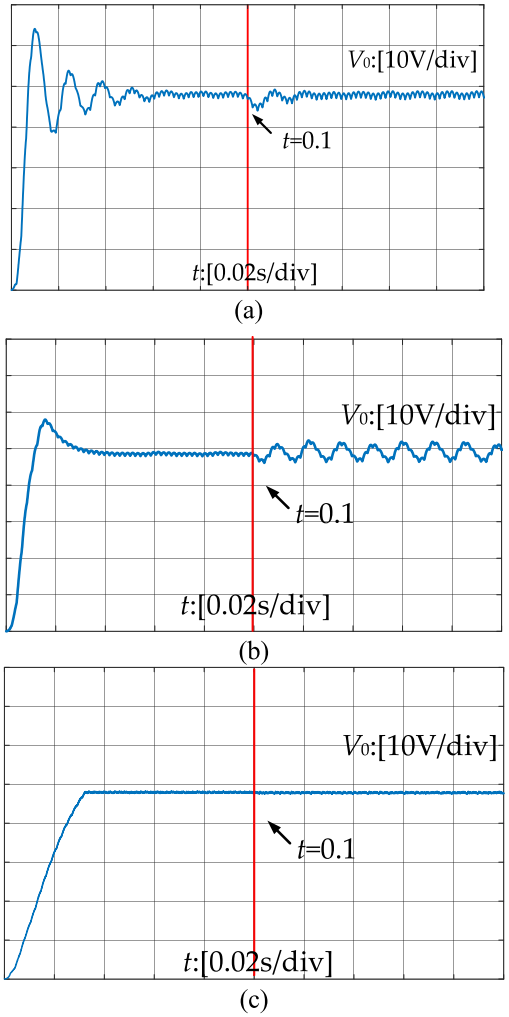

FIGURE 18. The simulation waveforms of the SR power generation system starting with variable loads; (a) The waveforms under PI control; (b) The waveforms under PT control; (c) The waveforms under FW-PT control.

environment. Likewise, the time when the output voltage in the case of applying the traditional PI control re-stabilized at 48V is about 0.025s. Moreover, the output voltage derived when applying FW-PT control reaches a steady state after 0.005s (about 2 wave heads) and can maintain a given voltage of 48V with a small output voltage ripple. The above analysis shows that the FW-PT control can start fast, and a fast response can be achieved within a certain range of variable load conditions, and the output voltage has a small ripple at the same time. The results are shown in Table 2.

Figure 19 shows the voltage waveforms of the SR power generation system that the load is changed from 12 Ω to 6 Ω at the instants of starting and changing loads under the traditional PI, PT and the FW-PT controls. The waveforms show the similar results to the first simulation. The results are shown in Table 3.

As shown in Figure 19, the waveforms show the similar results to the first simulation. The traditional PT control is not suitable for the SR power generation system under a

TABLE 2. The simulation results of the SR power generation system when the load is changed from 12 Ω to 10 Ω under three different control schemes.

Control schemes	Starting time (s)	Voltage ripple(12Ω)	Adjusting time (s)	Voltage ripple(10Ω)
PI	0.06	3.125%	0.020	3.755%
PT	0.04	2.083%	0.008	8.333%
FW-PT	0.03	1.041%	0.005	1.251%

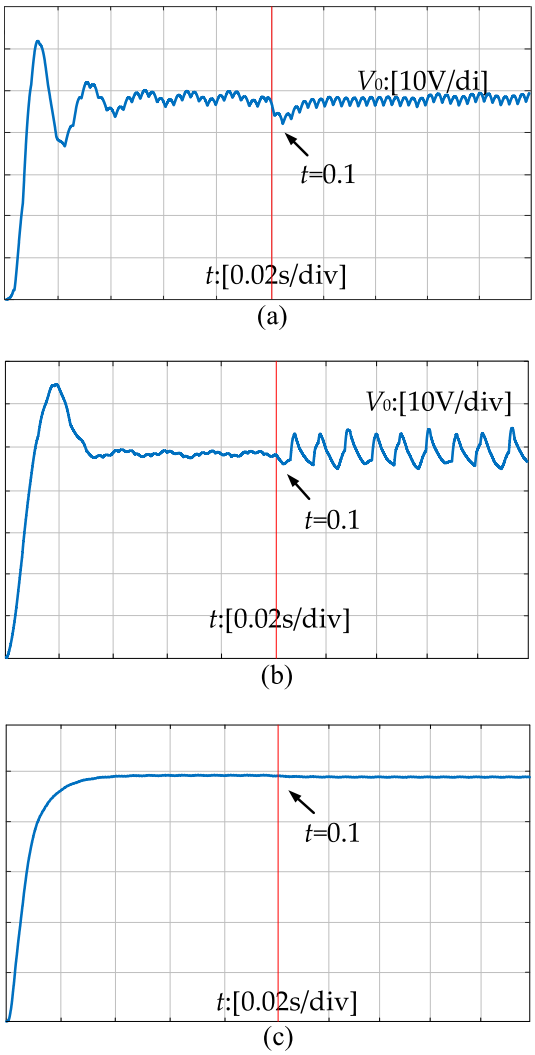

FIGURE 19. The simulation waveforms of the SR power generation system starting with variable loads; (a) The waveforms under PI control; (b) The waveforms under PT control; (c) The waveforms under FW-PT control.

variable load environment. The traditional PI control has a large overshoot and the robustness is better than PT control. The FW-PT control, which also has great robustness, can achieve a fast response within a certain range of variable load conditions and the output voltage has a small ripple at the same time.

Figure 20 shows the control signal of FW-PT control under the situation of variable loads. It can be seen that with the

TABLE 3. The simulation results of the SR power generation system when the load is changed from 12 Ω to 6 Ω under three different control schemes.

Control schemes	Starting time (s)	Voltage ripple(12Ω)	Adjusting time (s)	Voltage ripple(6Ω)
PI	0.06	4.583%	0.020	4.232%
PT	0.04	2.08%	0.008	13.8%
FW-PT	0.03	0.63%	0.005	0.58%

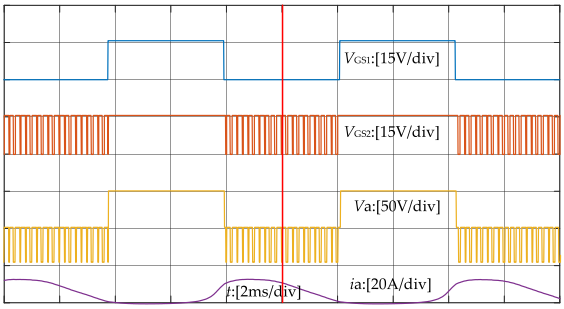

FIGURE 20. The control signal of FW-PT control under the condition of variable loads.

change of loads, the FW-PT control just adjusts the number of P_{H} and P_{L}, which can ensure that the system reaches a steady condition quickly.

The output power P_{out}, which is the difference between the generation power and the excitation power in an electric cycle, can be expressed as

$$P_{out} = \frac{N}{T}\left(-\frac{U}{\theta_c - \theta_{off}}\int_{\theta_{off}}^{\theta_3} i(\theta)\,d\theta - \frac{U}{\theta_{off} - \theta_{on}}\int_{\theta_{on}}^{\theta_{off}} i(\theta)\,d\theta\right) \quad (13)$$

Mean torque T_{ave}, which can be obtained by turning on period θ_{r} and electromagnetic torque T_{em}, is expressed as

$$T_{ave} = \frac{N}{\theta_r}\int_0^{\theta_r} T_{em}d\theta \quad (14)$$

System efficiency η for output power P_{out} and the ratio of the mechanical input power P_{in} can be expressed as

$$\begin{aligned}\eta &= \frac{P_{out}}{P_{in}} \times 100\% \\ &= \frac{P_{out}}{-T_{ave}\omega} \times 100\% \\ &= \frac{P_{out}}{-\frac{N}{\theta_r}\int_0^{\theta_r} T_{em}d\theta\omega} \times 100\%\end{aligned} \quad (15)$$

The efficiencies of the SR power generation system when the load is changed from 12 Ω to 6 Ω under three different control schemes are shown in Table 4.

It can be seen form the Table 4 that the efficiency of the SR power generation system with FW-PT control is better than the efficiency of the system with other two control strategies.

TABLE 4. The efficiencies of the SR power generation system when the load is changed from 12 Ω to 6 Ω under three different control schemes.

Control schemes	Efficiency (12Ω)	Efficiency (6Ω)
PI	81.3%	82.5%
PT	84.2%	84.6%
FW-PT	87.1%	87.8%

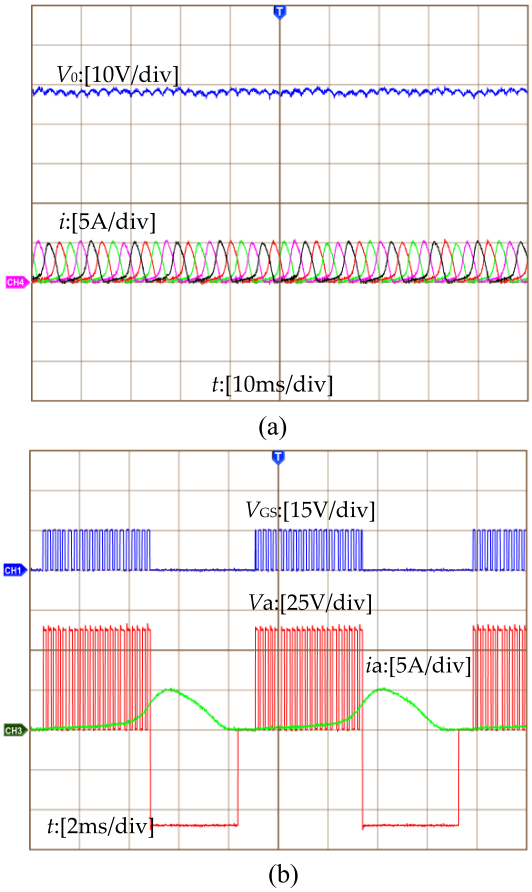

FIGURE 21. The experimental waveforms of SRG under the PID control; (a) The waveforms of output voltage V0 and phase currents; (b) The waveforms of control signal S1, voltage and current of phase A.

The above simulation results prove the feasibility of the FW-PT control proposed in this paper. Figure 21 shows the experimental waveforms of the SR power generation system with the traditional PID control. It can be seen that when the system reaches the steady state, the output voltage V_0 is about 48V, there is a large voltage ripple of V_0, and the amplitude of the phase current is 6A. Figure 21(b) shows the experimental waveforms of control signal, phase voltage and current of phase A, which agrees with the simulation results.

Figure 22 shows the experimental waveforms of the SR power generation system with the traditional PT control. It can be seen that the output voltage V_0 can be stabilized

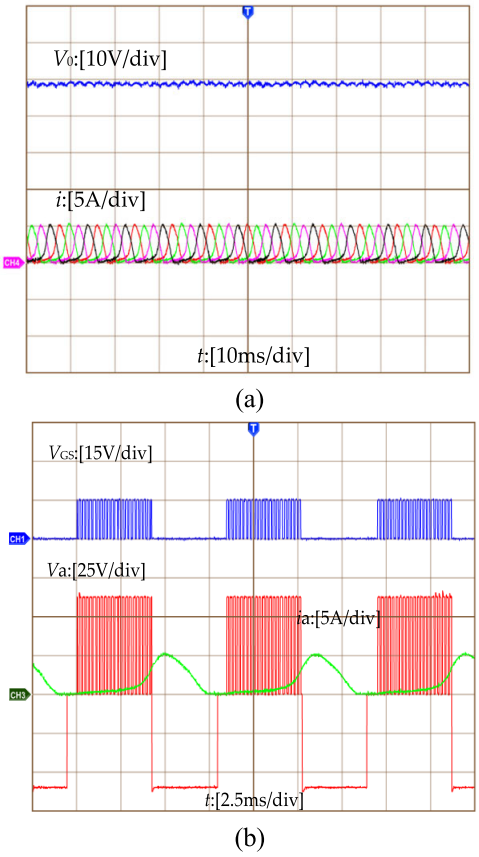

FIGURE 22. The experimental waveforms of the SR power generation system under the PT control. (a) The waveforms of output voltage V0 and phase currents; (b) The waveforms of control signal S1, voltage and current of phase A.

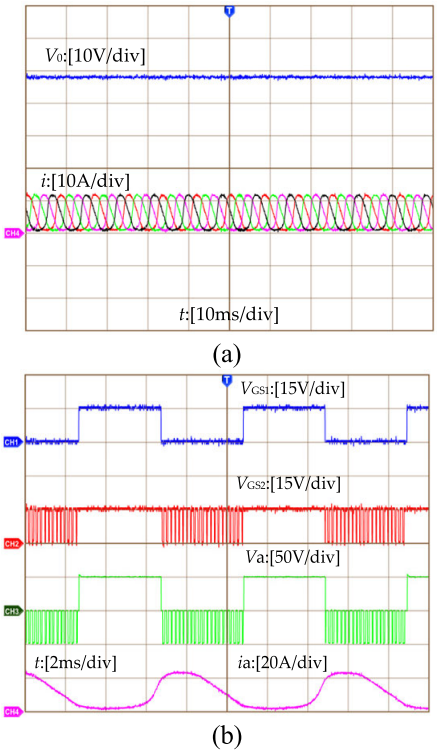

FIGURE 23. The experimental waveforms of the SR power generation system under the FW-PT control. (a) The waveforms of output voltage V0 and phase currents; (b) The waveforms of control signal S1, voltage and current of phase A.

at 48V, but there is still a large fluctuation. Compared with the traditional PI control, the output voltage ripple when applying the traditional PT control is smaller than the ripple under the traditional PI control. Figure 22(b) shows the experimental waveforms of control signal, phase voltage and current of phase A, which agrees with the simulation results.

Figure 23 shows the experimental waveforms of the SR power generation system with FW-PT control. It can be seen that the output voltage V_0 is stabilized at a given value of 48V and there is almost no ripple. Since the switches are fully turned on in the excited section, the amplitude of phase currents is increased to 12A and the waveforms remain symmetrical. The above analysis shows that the FW-PT control has obvious advantages in suppressing output voltage ripple compared to the traditional PI and PT controls. Figure 23(b) shows the experimental waveforms of control signal, phase voltage and current of phase A, which agrees with the simulation results.

Figure 24 shows the experimental waveforms of the output voltage of the SR power generation system with the three control methods. It can be seen that with PI control, the overshoot at the startup phase is large, and the output voltage V_0 reaches the steady state after 0.07s. Likewise, with the traditional PT control, due to the limitation of the high duty cycle pulse PH and the fact that there is no need for network compensation, the output voltage V_0 has a smaller overshoot at the startup phase, and 0.03s is needed to reach the steady state, and ripples still exist. Moreover, with FW-PT control, because the switches are fully turned on during the excitation phase, the SR power generation system can quickly establish the voltage. In the fly-wheeling phase, due to the limitation of the high power pulse P_H, the output voltage V_0 has no overshoot, and only 0.025s is needed to reach a stable state and the voltage ripple is almost 0V.

Figure 25 shows the experimental waveforms of the output voltage when the load changes in the case of applying the three control methods respectively for the SR power generation system. At time t_1, the load is abruptly changed from 12Ω to 10Ω. It can be seen that with the traditional PI control, after about 0.02s, the system reaches the steady state again, and the output voltage V_0 is stabilized at a given voltage of 48V. Similarly, with the traditional PT control, the system reaches the steady state after about 0.01s, and the voltage ripple is larger than before. Therefore, the traditional PT control does not meet the sudden change of the load of the SR power generation system. Furthermore, with the proposed FW-PT control, due to the full complete conduction in the excited phase, it provides sufficient energy for the fly wheeling of the SRG. Due to the switching of P_H and P_L, the SR power

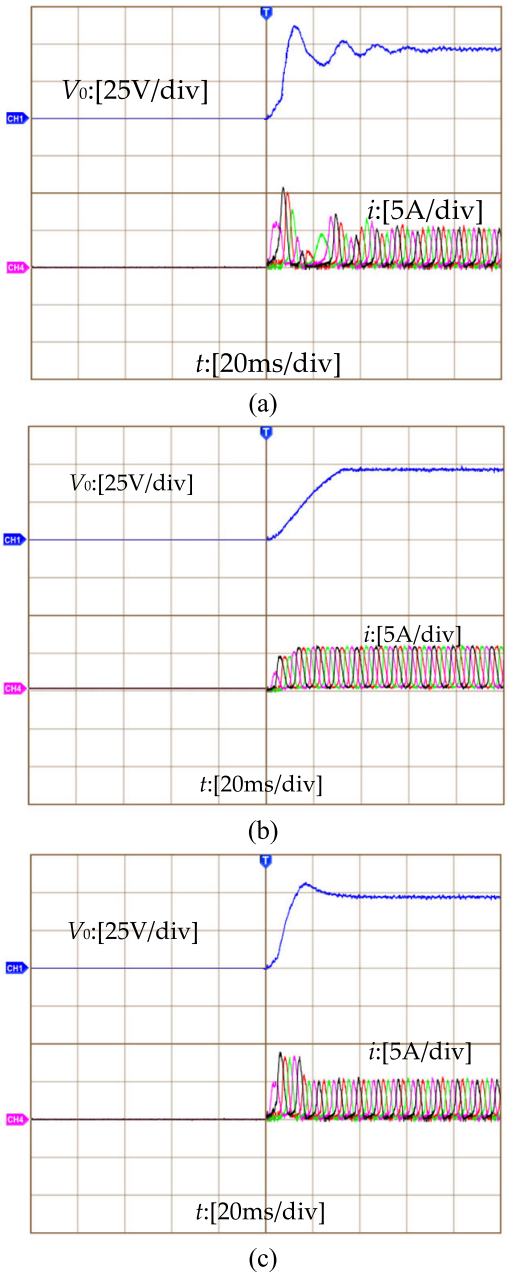

FIGURE 24. The experimental waveforms of the starting voltage in the SR power generation system; (a) The waveforms under PI control; (b) The waveforms under PT control; (c) The waveforms under FW-PT control.

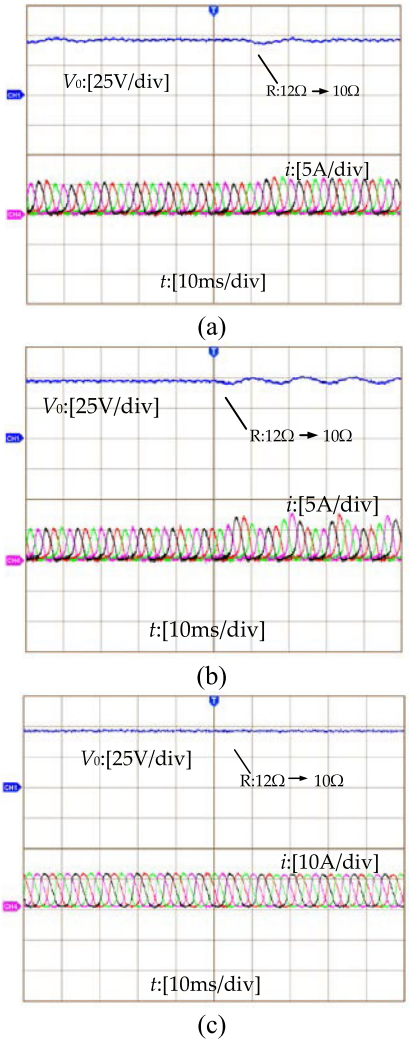

FIGURE 25. The experimental waveforms of the SR power generation system with variable loads; (a) The waveforms under PI control; (b) The waveforms under PT control; (c) The waveforms under FW-PT control.

TABLE 5. The experimental results of the SR power generation system when the load is changed from 12 Ω to 10 Ω under three different control schemes.

Control schemes	Starting time (s)	Voltage ripple(12Ω)	Adjusting time (s)	Voltage ripple(10Ω)
PI	0.070	5.208%	0.015	6.250%
PT	0.035	4.583%	0.009	10.421%
FW-PT	0.030	4.375%	0.003	4.479%

generation system has a certain capacity of variable loads, and after a short period of time, the output voltage can be re-stabilized at a given voltage of 48V, with a small ripple. The results are shown in Table 5.

Figure 26 shows the experimental waveforms of the SR power generation system that the load is changed from 12 Ω to 6 Ω at the instants of starting and changing loads under the traditional PI, PT and the FW-PT controls. The results are shown in Table 6.

As shown in Figure 26, when the load is changed from 12 Ω to 6 Ω, the SR power generation system with PI control can reach the steady state again. The system with PT control has worse robustness than the other two control schemes and the voltage ripple is much larger than before. It is obvious that system with FW-PT control has a certain capacity of variable loads, and after a short period of time, the output voltage can be re-stabilized at a given voltage of 48V, with a small ripple.

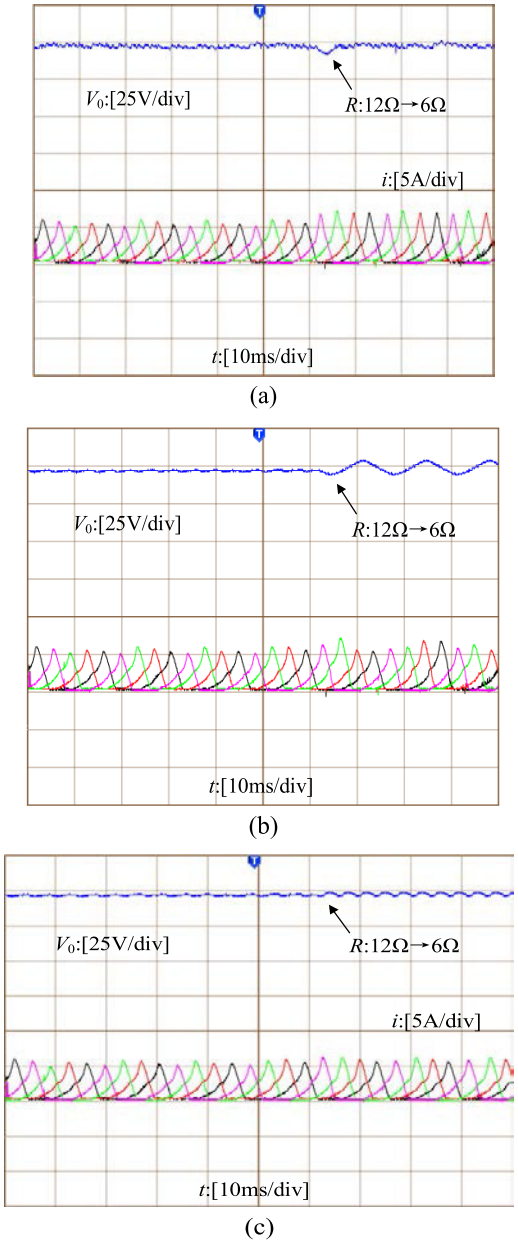

FIGURE 26. The experimental waveforms of the SR power generation system with variable loads; (a) The waveforms under PI control; (b) The waveforms under PT control; (c) The waveforms under FW-PT control.

TABLE 6. The experimental results of the SR power generation system when the load is changed from 12 Ω to 6 Ω under three different control schemes.

Control schemes	Starting time (s)	Voltage ripple(12Ω)	Adjusting time (s)	Voltage ripple(6Ω)
PI	0.070	5.208%	0.009	6.481%
PT	0.035	4.381%	0.006	17.292%
FW-PT	0.030	4.375%	0.003	5.021%

Figure 27 shows the control signal of FW-PT control with variable loads. The marshalling sequence of PH and P_L is changed. After changing the loads, the combination of

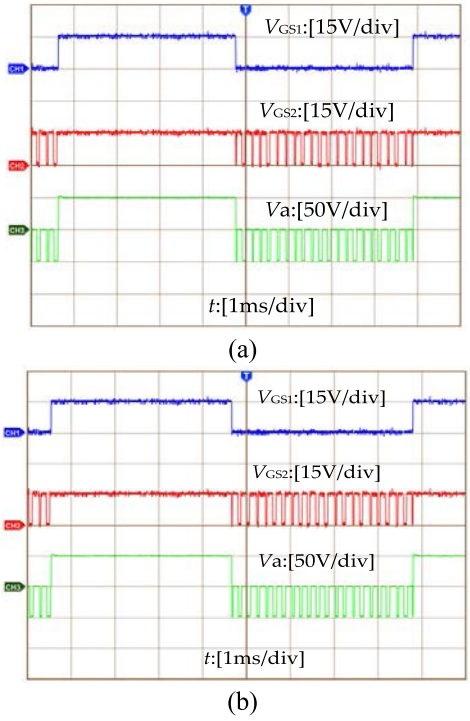

FIGURE 27. The experimental waveforms of control signal of FW-PT control with variable loads; (a) Control signal of FW-PT control before load changing; (b) Control signal of FW-PT control after load changing.

control signal transforms from "$P_L P_H P_H P_L P_H P_H P_H P_L P_H P_L$ $P_L P_H P_H P_L P_H P_H P_L P_H P_L P_H P_L$" to "$P_L P_L P_H P_H P_L P_L P_H$ $P_L P_L P_L$ $P_L P_H P_L P_H P_L P_H P_L P_L P_H P_L P_L$". By choosing the different number of P_H and P_L, the output voltage can be quickly adjusted by using FW-PT control.

V. CONCLUSION

Based on the traditional PT control, the FW-PT control method is proposed in this paper to improve the performance of the SR power generation system. It can be seen through experimental verification that, compared with the traditional SR power generation system with the PID and PT control methods, the FW-PT controlled SR power generation system has the following advantages:

(1) During the excited phase, with the full conduction of switches, the SR power generation system can quickly start and establish the bus voltage, and due to the limitation of the high duty cycle pulse P_H and no network compensation, the output voltage has no overshoot.

(2) The FW-PT control method regulates the fly-wheeling currents and selects the high and low duty cycle pulse trains according to the feedback value of the voltage in each phase, which can effectively suppress the ripple of the output voltage.

(3) The SR power generation system with FW-PT control has the good response capacity for variable loads. The number of high and low duty cycle pulse trains are selected according to the change in the load to ensure that the output

voltage is maintained at a given value and has better response characteristics.

In spite of the advantages mentioned above, the FW-PT control still needs further study. The optimization of output voltage is accompanied by the reduction of efficiency and application range of FW-PT control is small. Next, further research will be conducted on the above two issues.

REFERENCES

[1] J. Cai and Z. Deng, "A joint feature position detection-based sensorless position estimation scheme for switched reluctance motors," *IEEE Trans. Ind. Electron.*, vol. 64, no. 6, pp. 4352–4360, Jun. 2017.
[2] J. Ye, B. Bilgin, and A. Emadi, "An extended-speed low-ripple torque control of switched reluctance motor drives," *IEEE Trans. Power Electron.*, vol. 30, no. 3, pp. 1457–1470, Mar. 2015.
[3] H. Cheng, H. Chen, Q. Wang, S. Xu, and S. Yang, "Design and control of switched reluctance motor drive for electric vehicles," in *Proc. 14th Int. Conf. Control, Automat., Robot. Vis. (ICARCV)*, 2016, pp. 1–6.
[4] R. Cardenas, R. Pena, M. Perez, J. Clare, G. Asher, and P. Wheeler, "Control of a switched reluctance generator for variable-speed wind energy applications," *IEEE Trans. Energy Convers.*, vol. 20, no. 4, pp. 781–791, Dec. 2005.
[5] C. Gan, J. Wu, Y. Hu, S. Yang, W. Cao, and J. L. Kirtley, "Online sensorless position estimation for switched reluctance motors using one current sensor," *IEEE Trans. Power Electron.*, vol. 31, no. 10, pp. 7248–7263, Oct. 2016.
[6] E. Sunan, F. Kucuk, K. S. Raza, H. Goto, H. J. Guo, and O. Ichinokura, "Torque ripple minimization and maximum power point tracking of a permanent magnet reluctance generator for wind energy conversion system," *J. Renew. Sustain. Energy*, vol. 5, no. 1, pp. 781–1515, 2013.
[7] M. Cui, X. Zan, F. Chi, M. Wang, and D. Yu, "Research on optimization of SRG power generation performance based on the QBC with coupled inductor," in *Proc. Automat. Congr. (CAC)*, 2017, pp. 3481–3486.
[8] H. Le-Huy and M. Chakir, "Optimizing the performance of a switched reluctance generator by simulation," in *Proc. 19th Int. Conf. Elect. Mach.*, Sep. 2010, pp. 1–6.
[9] Y. Z. Liu, Z. Zheng, Z. J. Sheng, B. J. Fan, and J. L. Song, "Study of control strategy for status switching of switched reluctance starter/generator," *Electr. Mach. Control*, vol. 19, pp. 57–63, Oct. 2015.
[10] E. S. L. Oliveira, M. L. Aguiar, and I. N. D. Silva, "Strategy to control the terminal voltage of a SRG based on the excitation voltage," *IEEE Latin Amer. Trans.*, vol. 13, no. 4, pp. 975–981, Apr. 2015.
[11] B. Shao and A. Emadi, "A digital control for switched reluctance generators," in *Proc. IEEE Int. Conf. Mechatronics*, Apr. 2011, pp. 182–187.
[12] X. Zan, M. Cui, R. Xu, and K. Ni, "Improvement of the response speed for switched reluctance generation system based on modified PT control," *Energies*, vol. 11, no. 8, p. 2049, 2018.
[13] F. Luo and D. Ma, "An integrated switching DC–DC converter with dual-mode pulse-train/PWM control," *IEEE Trans. Circuits Syst. II, Exp. Briefs*, vol. 56, no. 2, pp. 152–156, Feb. 2009.
[14] J. Wang, J. Xu, G. Zhou, and B. Bao, "Pulse-train-controlled CCM buck converter with small ESR output-capacitor," *IEEE Trans. Ind. Electron.*, vol. 60, no. 12, pp. 5875–5881, Dec. 2013.
[15] J.-P. Xu, Q.-B. Mu, J.-P. Wang, and M. Qin, "Output voltage ripple of pulse train controlled DCM buck converter," *Electr. Mach. Control.*, vol. 14, pp. 1–6, May 2010.
[16] F. S. Kang and S. J. Park, "A linear encoder using a chiaroscuro and its extension to switched reluctance motor drive," *Energy Convers. Manage.*, vol. 46, no. 7, pp. 1119–1128, 2005.
[17] A. Chiba, Y. Takano, M. Takeno, T. Imakawa, N. Hoshi, M. Takemoto, and S. Ogasawara, "Torque density and efficiency improvements of a switched reluctance motor without rare-earth material for hybrid vehicles," *IEEE Trans. Ind. Appl.*, vol. 47, no. 3, pp. 1240–1246, May/Jun. 2011.
[18] N. S. Gameiro and A. J. M. Cardoso, "A new method for power converter fault diagnosis in SRM drives," *IEEE Trans. Ind. Appl.*, vol. 48, no. 2, pp. 653–662, Mar./Apr. 2012.
[19] E. Sunan, K. S. M. Raza, H. Goto, H.-J. Guo, and O. Ichinokur, "Instantaneous torque ripple control and maximum power extraction in a permanent magnet reluctance generator driven wind energy conversion system," in *Proc. 19th Int. Conf. Elect. Mach.*, Sep. 2010, pp. 1–6.
[20] P. J. dos Santos Neto, T. A. dos Santos Barros, M. V. de Paula, R. R. de Souza, and E. R. Filho, "Design of computational experiment for performance optimization of a switched reluctance generator in wind systems," *IEEE Trans. Energy Convers.*, vol. 33, no. 1, pp. 406–419, Mar. 2018.
[21] Z. Zhang, P. Zhaoyu, and G. Feng, "Research on new control model for switched reluctance motor," in *Proc. Int. Conf. Comput. Appl. Syst. Modeling*, vol. 10, 2010, pp. 198–202.
[22] D. A. Torrey, "Switched reluctance generators and their control," *IEEE Trans. Ind. Electron.*, vol. 49, no. 1, pp. 3–14, Feb. 2002.

XIAOSHU ZAN received the B.Eng. and Ph.D. degrees from the School of Information and Electrical Engineering, China University of Mining and Technology, Xuzhou, China, in 2003 and 2011, respectively. In 2001, he joined the School of Information and Electrical Engineering, China University of Mining and Technology as a Lecturer. His research interests include switched reluctance motor, power electronics, and renewable power generation. He has published more than ten articles in these areas.

KAI NI (S'17) was born in Jiangsu, China. He received the B.Eng. (Hons.) and Ph.D. degrees in electrical engineering from the University of Liverpool, Liverpool, U.K., in 2016 and 2019, respectively. He joined the School of Electrical and Electronic Engineering with the Huazhong University of Science and Technology, in December 2019, as a Postdoctoral Researcher. His research interests include modeling, control and stability analysis of doubly-fed induction machines, power electronic converters, and shipboard power systems.

WENYUAN ZHANG was born in Shandong, China. He is currently pursuing the M.S. degree in electrical engineering from the China University of Mining and Technology. His current research interests include operation and control of switched reluctance motors, current-sharing control of switched reluctance generators in parallel and novel power converters.

ZHIKAI JIANG was born in Shandong, China. He received the B.Eng. degree from the China University of Mining and Technology, where he is currently pursuing the M.S. degree in electrical engineering. His current research interests include operation and control of switched reluctance motor systems, power electronic converters, and electric drives.

MINGLIANG CUI was born in Jiangsu, China. He is working for the State Grid Dongtai County Electric Power Supply Company. His current research interests include operation and control of switched reluctance motor systems, power electronics, renewable energy, and renewable power generation.

DONGSHENG YU (M'14) received the B.Eng. and Ph.D. degrees from the School of Information and Electrical Engineering, China University of Mining and Technology, Xuzhou, China, in 2005 and 2011, respectively. From 2009 to 2010, he was a Visiting Student with The University of Western Australia, Australia, where he was an Endeavour Research Fellow, in 2014. He is currently an Associate Professor with the School of Information and Electrical Engineering, China University of Mining and Technology. He has owned five provincial level awards for outstanding works in the teaching and research. His research interests include power electronics, renewable energy, electric drives, nonlinear dynamics, and memristive systems. He has published two books and more than 30 articles in these areas.

RONG ZENG (S'10–M'17) received the M.Sc. degree in electrical engineering from Zhejiang University, Hangzhou, China, in 2011, and the Ph.D. degree in electrical engineering from the University of Strathclyde, Glasgow, U.K., in 2015.

He is currently working as a Technical Professional Staff with the Oak Ridge National Laboratory, Power Electronics and Electric Machine Group, TN, USA. His research interests include high power converters for HVDC application, grid integration of renewable energy systems, and wireless charging for electric vehicle application.